Review Article

Magnetic resonance imaging (MRI)-based radiomics for prostate cancer radiotherapy

Fei Yang[1], John C. Ford[1], Nesrin Dogan[1], Kyle R. Padgett[1,2], Adrian L. Breto[1], Matthew C. Abramowitz[1], Alan Dal Pra[1], Alan Pollack[1], Radka Stoyanova[1]

[1]Department of Radiation Oncology, [2]Department of Radiology, University of Miami Miller School of Medicine, Miami, FL 33136, USA

Contributions: (I) Conception and design: F Yang, JC Ford, A Pollack, R Stoyanova; (II) Administrative support: A Pollack; (III) Provision of study materials or patients: MC Abramowitz, A Dal Pra, A Pollack; (IV) Collection and assembly of data: F Yang, JC Ford, N Dogan, KR Padgett, AL Breto, R Stoyanova; (V) Data analysis and interpretation: F Yang, JC Ford, R Stoyanova; (VI) Manuscript writing: All authors; (VII) Final approval of manuscript: All authors.

Correspondence to: Radka Stoyanova, PhD. Department of Radiation Oncology, University of Miami Miller School of Medicine, 1475 NW 12th St., Miami, Florida 33136, USA. Email: RStoyanova@med.miami.edu.

Abstract: In radiotherapy (RT) of prostate cancer, dose escalation has been shown to reduce biochemical failure. Dose escalation only to determinate prostate tumor habitats has the potential to improve tumor control with less toxicity than when the entire prostate is dose escalated. Other issues in the treatment of the RT patient include the choice of the RT technique (hypo- or standard fractionation) and the use and length of concurrent/adjuvant androgen deprivation therapy (ADT). Up to 50% of high-risk men demonstrate biochemical failure suggesting that additional strategies for defining and treating patients based on improved risk stratification are required. The use of multiparametric MRI (mpMRI) is rapidly gaining momentum in the management of prostate cancer because of its improved diagnostic potential and its ability to combine functional and anatomical information. Currently, the Prostate Imaging, Reporting and Diagnosis System (PIRADS) is the standard of care for region of interest (ROI) identification and risk classification. However, PIRADS was not designed for 3D tumor volume delineation; there is a large degree of subjectivity and PIRADS does not accurately and reproducibly elucidate inter- and intra-lesional spatial heterogeneity. "Radiomics", as it refers to the extraction and analysis of large number of advanced quantitative radiological features from medical images using high throughput methods, is perfectly suited as an engine to effectively sift through the multiple series of prostate mpMRI sequences and quantify regions of interest. The radiomic efforts can be summarized in two main areas: (I) detection/segmentation of the suspicious lesion; and (II) assessment of the aggressiveness of prostate cancer. As related to RT, the goal of the latter is in particular to identify patients at high risk for metastatic disease; and the aim of the former is to identify and segment cancerous lesions and thus provide targets for radiation boost. The article is structured as follows: first, we describe the radiomic approach; and second, we discuss the radiomic pipeline as tailored for RT of prostate cancer. In this process we summarize the current efforts and progress in integrating mpMRI radiomics into the radiotherapeutic management of prostate cancer with emphasis placed on its role in treatment target definition, treatment plan strategizing, and prognostic assessment. The described concepts, methods and tools are not currently applicable to the radiation oncology practice outside of the research setting. More data are required in the form of clinical trials to assess the robustness of radiomics-based predictive models, and to maximize the efficacy of these models.

Keywords: Prostate cancer; radiomics; multiparametric magnetic resonance imaging (mpMRI); radiotherapy (RT)

Submitted Feb 17, 2018. Accepted for publication Jun 05, 2018.
doi: 10.21037/tau.2018.06.05
View this article at: http://dx.doi.org/10.21037/tau.2018.06.05

Introduction

In 2018, approximately 164,690 men in US will be diagnosed with prostate cancer and approximately 29,500 men will die of the disease (1). About half of these patients will be treated with radiotherapy (RT). Prostate cancer has a long natural history and the consequences of local persistence may not be realized for many years; but the relationship between local persistence, biochemical failure, distant metastasis and mortality has been established (2-7). There is significant evidence in support of doses of 76 Gy or higher for primary treatment of localized prostate, and doses above 80 Gy increase biochemical control (8-10). There is also some evidence to support the theory that regions in the prostate with the greatest tumor burden are at highest risk of harboring persistent disease after RT (6,7,11,12). Limiting the highest radiation doses to the gross tumor volume (GTV), as opposed to whole prostate, is hypothesized to result in equivalent tumor control without increasing side effect (13,14). A recent meta-analysis of 22 published studies describing 1,378 patients treated with radiation boost to the dominant intraprostatic lesion (MRI-visible GTV), while acknowledging the limitations inherent due to the heterogeneity of the study, concludes that there are encouraging results for focal dose escalation with acceptable short- to medium-term side effects and biochemical disease control rates (15). While contemporary treatment methods, such as intensity-modulated RT (IMRT), are used to deliver radiation with high accuracy, defining the position and the extent of the tumor is still quite challenging. Other issues in the treatment of the RT patient include the choice of the RT technique (hypo- or standard fractionation) and the use and length of androgen deprivation therapy (ADT) (16,17).

In this review, we summarize the efforts in quantitative MRI analysis of the prostate to: (I) improve tumor targeting in RT; and (II) optimize the treatment strategies by better risk stratification. Multiparametric MRI (mpMRI) is becoming widely integrated in the daily management of prostate cancer and used for detection, localization and staging of the disease. mpMRI consists of sequences for dynamic contrast enhanced-MRI (DCE-MRI), diffusion via diffusion-weighted imaging (DWI) and anatomical information [T2-weighted (T2w) MRI] (18,19).

Currently, the Prostate Imaging, Reporting and Diagnosis System (PIRADS) is the standard of care for region of interest (ROI) identification and risk classification (20,21). PIRADS was not designed for a 3D tumor volume delineation. Typically, a lesion is described in the radiologist report by its location and PIRADS score assigned (1 to 5). For GTV delineation, the precise contours of the tumor are needed. Further, the five-score system does not tap into the wealth of quantitative imaging information contained in the multiple sequences of mpMRI, nor does it elucidate intralesional spatial heterogeneity.

"Radiomics", as it refers to the extraction and analysis of large number of advanced quantitative imaging features from medical images using high throughput methods (22,23), can probe and capture inherent tissue characteristics in the multiple series of prostate mpMRI and quantify the regions of interest (24). The radiomics efforts can be summarized in two main areas: (I) detection/segmentation of the suspicious lesion; and (II) assessment of the aggressiveness of prostate cancer. As related to RT, the goal of the latter is in particular to identify patients at high risk for metastatic disease; and the aim of the former is to identify and segment cancerous lesions and thus provide targets for radiation boost. The remainder of the paper is structured as follows: first, we give an overview of the radiomic approach. Then, we discuss the radiomic pipeline as tailored for RT of prostate cancer. Next, we summarize the current efforts in RT of prostate cancer for automatic delineation of GTV and tumor aggressiveness assessment. Furthermore, we introduce delta radiomics as promising tool for RT outcome prediction in prostate cancer. Finally, we conclude the review by highlighting the challenges and potentials of radiomics in RT management of prostate cancer.

Radiomics

Radiomics, as applied to oncology, is a type of quantitative medical image analysis that exploits image "features" as biomarkers to aid in tumor detection and localization as well as prediction of treatment response. The quantitative image characteristics that serve as radiomic features, some of which cannot be discerned by eye of even the expert radiologist, range broadly from semantic to morphological to statistical to transform-based in nature (25-27). In contrast to biopsy procedures, non-invasive imaging methods such as CT, PET and MRI afford assessment of spatial variability throughout the entire three-dimensional volume of the tumor, which is very important as tumor heterogeneity is commonly associated with malignancy and aggressiveness (25,28-30). In addition to tumor assessment, radiomics analysis can be applied to nearby organs at risk to predict RT-related

normal tissue toxicity and guide adaptive treatment (31). Thus, radiomics is emerging as a promising methodology in RT towards the goal of providing precision medicine and stratifying cancer patients for personalized care.

A radiomics framework for a given tumor site has at its foundation a large, often multi-institutional, database of standard of care radiologic images from which image feature-based predictive models of patient outcome can be built, along with patient clinical data. The radiomics workflow involves image acquisition, followed by manual or automated contouring of regions of interest, feature extraction, and finally creation of predictive models through correlation of image features with clinical data, e.g., diagnostic status, treatment response, and possibly genomics data (25,29). As pointed out by Gillies *et al.* (25), radiomics is a natural extension of computer-aided diagnosis and detection (CAD) systems; however, whereas CAD systems are aimed at providing a specific answer (e.g., detection of disease), radiomics provides a process for mining a large number (typically hundreds or thousands) of quantitative image features that can subsequently be mined for hypothesis generation and/or testing. Since the number of features often exceeds the number of patients, selection of only those features that contribute to clinical prediction is warranted. This selection entails, in part, identification of features that are robust, reproducible and repeatable, and not correlated with one another. Once the subset of useful features has been identified, they are then input to a model that serves to classify the patient, e.g., malignant versus benign disease, responder versus non-responder. Supervised classifier models, which use one data set of images and related clinical data to train the model, and another data set to validate and test the model, include methods such as random forest (based on decision trees), support vector machines, and convolutional neural networks. Unsupervised classifier models, such as consensus clustering, seek to categorize cancer subtypes in a patient population with no a priori clinical outcome data. For an excellent review of feature selection and classifier modeling, please refer to Avanzo *et al.* (28), and references contained therein. For a comprehensive review of the computational resources available for building a radiomics framework, see Court *et al.* (32).

Radiomics pipeline in RT

The steps of the radiomics process for analysis of prostate mpMRI are shown in *Figure 1*.

mpMRI of the prostate

mpMRI exam of the prostate typically includes acquisition of T2w, DWI and DCE-MRI data. An apparent diffusion coefficient (ADC) map is calculated on the MRI scanner's console. The acquired images are transferred to an image processing station. A variety of commercial medical image computing platforms are currently used in RT, e.g., MIM (MIM, Cleveland, OH, USA), Mirada (Mirada Medical USA, Denver, CO, USA), and Velocity (Varian Medical Systems, Palo Alto, CA, USA). These commercial platforms are useful for image display, volume segmentation, and image registration, but currently do not support radiomic analysis.

Volume segmentation

Accurate identification of volume of interest (VOI) is the most critical and challenging step in the radiomics process. It is critical in that it defines the spatial context and character from which the subsequent feature data are derived. It is challenging for the reason that prostate is an organ featuring unique anatomical traits that require detailed segmentation and oftentimes are accompanied with rather indistinct margins in its radiological manifestations. The peripheral zone (PZ) and the transition zone (TZ) are in generally considered separately in identifying prostate habitats given the reason that they are associated with different imaging characteristics on T2w and ADC. The peri-urethral zone (PUZ), featuring high vascularity and yielding false positives on DCE, is commonly excluded from the VOI. Furthermore, regions of normal appearing tissue (NAT) in PZ and TZ need to be identified. Although efforts have been made for automation or semi-automation of this process, manual delineation of tumor VOI is still the standard clinical routine in RT of patients with prostate cancer. Aside from being time-consuming and resource-demanding, manual contouring is well recognized to be susceptible to intra-operator and inter-operator variability (18,33).

Another aspect that makes VOI identification in prostate cancer challenging and somewhat unique is that segmentation is typically done within the context of mpMRI setting. The suspicious lesions are generally defined by aid of combination of co-registered image data from different modalities with each offering a piece of orthogonal information. In mpMRI, T2w provides superior

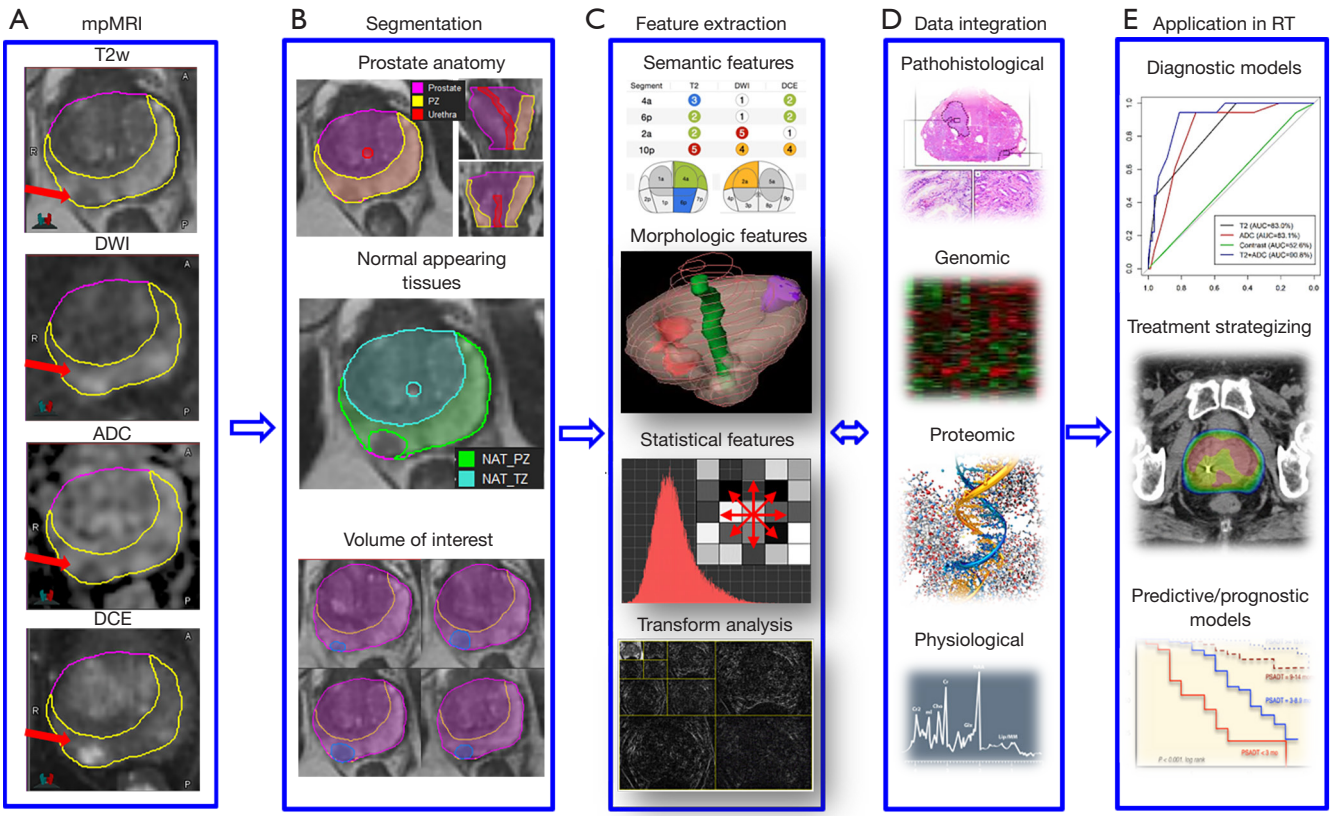

Figure 1 mpMRI radiomics in prostate RT. (A) mpMRI exam of the prostate typically includes acquisition of T2-weighted (T2w), diffusion-weighted imaging (DWI) and the associated apparent diffusion coefficient (ADC) map and dynamic contrast enhanced (DCE)-MRI. In this panel the T2w, DWI at high b-value (1,000 s/mm^2), ADC and the early enhancing image in the DCE-MRI from radiotherapy patient is shown. The red arrows indicate a tumor in the peripheral zone (PZ). The tumor appears darker on T2w, brighter on the high b-value DWI and it is characterized with reduced diffusion (ADC) and increased perfusion (DCE-MRI); (B) segmentation of volumes of interest (VOI) in prostate cancer radiotherapy generally involves identification of prostate, urethra, PZ, transition zone (TZ), as shown in the top panel, and differentiation of normal appearing tissues (NAT) in PZ and TZ, as shown in the middle panel, along with delineation of the gross tumor volume (GTV) in 3D, as shown in the bottom panel; (C) radiomics features extracted from prostate mpMRI can be grouped into four major categories related, respectively, to semantic, morphological, statistical, and transform analysis. Semantic features refer to quantitative descriptors derived by the radiologists empirically when assessing mpMRI, morphological features are measures of geometrical shape and physical composition of the segmented VOIs, statistical features quantify the gray level intensity distribution and/or spatial relations between image voxels inside VOIs, and transform-based features depict repetitive or non-repetitive spatial patterns through mathematical transformation to the segmented image content; (D) to achieve holistic models, radiomics features should be integrated with other available biomarkers, such as data from clinical records, genomic profiling, proteomic screening, and physiological analysis; (E) application of integrated data/models could span the entire range of radiotherapy for prostate cancer, from aiding in diagnostic establishment to facilitating patient-individualized treatment strategizing to improving predictive and prognostic accuracy.

soft tissue contrast and clear delineation of prostatic zonal anatomy, DCE takes advantage of vascular difference between malignant lesions and surrounding prostatic tissue to facilitate target identification, and ADC is associated with the density of diffusion barriers and exploits the higher cellular density and more complex intracellular microstructure in malignant lesions to differentiate benign prostatic tissue. The general practice is to consider the volumes of intersection between the corresponding data from DCE and ADC for lesion definition (34).

Table 1 Classification of radiomic features

Category	Encoding scheme and technique
Semantic	Prostate Imaging Reporting and Data System (PIRADS)
Morphological	First order geometric descriptions
	Higher order geometric descriptions
	❖ Minkowski functionals
	❖ Fractal dimension
Statistical	First order statistics
	❖ Gray-level intensity histogram (GLIH)
	Higher order statistics
	❖ Gray-level co-occurrence matrices (GLCOM); gray-level neighborhood difference matrices (GLNDM); gray-level run length matrices (GLRLM); gray-level size zone matrices (GLSZM)
Transform-based	Fourier transform
	Gabor transform
	Wavelet transform
	Laplacian transform of Gaussian bandpass filters

Radiomics features

From the identified tumor volumes, various quantitative radiologic features can be derived; thus, forms the engine of radiomic analysis for prostate cancer. Currently available radiomic features for prostate cancer can be grouped into four major categories: (I) semantic; (II) morphological; (III) statistical; (IV) transform-based (*Table 1*). Semantic features refer to a finite series of quantitative descriptors derived empirically by the radiologists when assessing mpMRI for improved detection, location, and risk stratification in patients suspected with prostate cancer, such as those defined in PIRADS (21). Morphological features describe the shape and physical composition of the segmented volumes. Features of this category range from simple first order geometric descriptors, such as volume and maximum diameter, to higher order topographical measures such as the Minkowski functionals featuring compactness, complexity, curvatures, and Euler number, etc. (35,36) and fractal dimensions that provide a measure of "overall roughness of local heterogeneities" (37). As to the statistical features, they can be further classified into first order and higher order statistical measures. First-order statistical features are related to the intensity histogram of image voxels within the segmented volumes and typically involve standard deviation, skewness, kurtosis, energy, and entropy with each characterizing the intensity histogram from the aspect of dispersion, symmetry, peakedness, uniformity, and randomness, respectively. Higher order statistical features consist of various textural parameters derived based on different encoding schemes including gray-level co-occurrence matrices (GLCOM), gray-level neighborhood difference matrices (GLNDM), gray-level run length matrices (GLRLM), and gray-level size zone matrices (GLSZM), amongst others. GLCOM-based textural parameters describe local spatial properties of the segmented volumes through examining the joint occurrence probability of one gray-level value relative to another at given linear displacements (38). For example, contrast measures the frequency of co-occurring local intensity variations. Correlation quantifies the spatial frequency of linear dependence of gray-levels. Energy describes the homogeneity of a region through co-occurring gray-level values; lower energy indicates fewer co-occurring gray-levels. GLNDM-based features exploit visual perceptual property of textures by discerning the spatial details of the segmented volumes in terms of the gray-level difference between voxels and their local neighborhoods (39). Coarseness is a measure of average difference between the

Table 2 Summary of representative higher order statistical radiomic features

Encoding scheme	Feature
Gray-level intensity histogram (GLIH)	Standard deviation
	Skewness
	Kurtosis
	Energy
	Entropy
Gray-level co-occurrence matrix (GLCOM)	Autocorrelation
	Contrast
	Correlation
	Dissimilarity
	Energy
	Entropy
	Homogeneity
Gray-level neighborhood difference matrix (GLNDM)	Coarseness
	Contrast
	Busyness
	Complexity
	Strength
Gray-level run length matrix (GLRLM)	Short runs emphasis
	Long runs emphasis
	Low gray-level runs emphasis
	High gray-level runs emphasis
	Short runs low gray-level emphasis
	Short runs high gray-level emphasis
	Long runs low gray-level emphasis
	Long runs high gray-level emphasis
	Gray-level non-uniformity
	Run length non-uniformity
	Run percentage
Gray-level size zone matrix (GLSZM)	Short zones emphasis
	Large zones emphasis
	Low gray-level zones emphasis
	High gray-level zones emphasis
	Short zones low gray-level emphasis
	Short zones high gray-level emphasis
	Large zones low gray-level emphasis
	Large zones high gray-level emphasis
	Gray-level non-uniformity
	Zone size non-uniformity
	Zone percentage

center voxel and its neighborhoods and is an indication of the spatial rate of change in gray levels. Busyness measures the spatial frequency of intensity changes between neighboring regions. An image is considered complex when there are multifold primitive components, i.e., the image is non-uniform and there are rapid changes in gray level intensity. GLRLM-based and GLSZM-based features quantify the spatial frequency of contiguous sets of constant gray level voxels within segmented volumes via quantifying the connectivity along specified directions or in all directions (40,41). Short runs emphasis and short zones emphasis assess the frequency of occurrence of short runs and small zones of the same gray-levels within the segmented VOI, with greater values indicative of more fine textural structures. Long runs low gray-level emphasis and large zones low gray-level emphasis track the frequency of occurrence of identical gray-levels in a direction or the frequency of similar sized zones of low gray-levels, with greater values indicative of more coarse structural textures. For a list of representative higher order statistical radiomic features, please refer to *Table 2*. And lastly, transform-based features depict repetitive or non-repetitive spatial patterns through imposing kernel functional transformation to the segmented image content. Some of the popularly used transformation are Fourier transform, Gabor transform, wavelet transform, Laplacian transforms of Gaussian bandpass filters (42-44).

Radiomics for RT applications

While most of the prostate cancer MRI-radiomics studies are not directly related to RT, the methods summarized below can be adopted and translated for RT applications. We describe the papers, grouped in two major groups: (I) GTV delineation; and (II) cancer aggressiveness. This summary is updated from our 2016 radiomics review (26) with special emphasis on approaches developed specifically for RT.

Delineation of prostate cancer lesions

The algorithms for automatic identification of the prostate cancer are summarized in *Table 3*. Madabhushi *et al.* (45) presented a method for detecting prostate cancer from high resolution MRI of prostatectomy samples. Lopes *et al.* (37) used fractal analysis to classify voxels as tumor or non-tumor on prostate T2w of 27 patients. Fractal analysis employed in their study combined fractal dimensions

Table 3 Summary of radiomics manuscripts related to automatic segmentation of GTV

Reference	Volumes	Modality	Feature category*
Madabhushi *et al.*, 2005 (45)	Prostate, ROI	T2w	Statistical; transform-based
Lopes *et al.*, 2011 (37)	NAT, ROI	T2w	Morphological; statistical
Cameron *et al.*, 2015 (46)	ROI	T2w; ADC; DWI**	Semantic; morphological; statistical
Shiradkar *et al.,* 2016 (47)	ROI	T2w; ADC; DWI	Morphological; statistical; transform-based

*, see *Table 1* for feature descriptions; **, correlated diffusion imaging (CDI) and individual b-value images are used. GTV, gross tumor volume; NAT, normal appearing tissues; ROI, region of interest; ADC, apparent diffusion coefficient; T2w, T2-weighted; DWI, diffusion-weighted imaging.

with multifractal spectra indices derived based on multi-fractional Brownian motion (mBm). The former provides a measure of global heterogeneity while the latter capture local heterogeneities. Cameron *et al.* (46) study provided a computer-aided detection of the prostate cancer using semantic, morphological and statistical features.

Shiradkar *et al.* (47) presented a RT planning framework to create targeted focal treatment plans. This framework utilized radiomics based detection of targeting cancerous prostate lesions on mpMRI using a statistical feature enabled machine learning classifier. Using a retrospective dataset of 23 patients from two institutions, target volumes, organs at risk and transference tissue from MRI were deformably-mapped onto CT. Eleven patients from one institution were used to train a radiomics classifier for predicting prostate lesions in 12 patients from a second institution. Brachytherapy and external beam treatment plans for both focal and whole prostate gland with focal boost were generated based on the radiomics detected lesions. Comparisons between radiomics based focal versus conventional plans showed better sparing of organs at risk using focal treatment plans.

Prostate cancer aggressiveness

Studies that aim to utilize radiomics to discriminate between low and high-risk cancer are summarized in *Table 4*. There is also a series of papers dedicated to diagnosis of a lesion, i.e. whether a lesion, usually manually contoured, is cancerous or not (54-58). These developments are outside of the scope of this review.

Wibmer *et al.* (48) investigated higher order statistical features of prostate mpMRI for diagnosis purposes. In the follow-up study by Fehr *et al.* (50) on the same cohort of patients used first-order statistical features to discriminate Gleason score (GS) (3+4) =7 versus GS (4+3) =7. Vignati *et al.* (49) used statistical features related to gray-level co-occurrence matrices including contrast and homogeneity extracted from T2w and ADC to predict prostate cancer aggressiveness.

In Nketiah *et al.* (51) higher statistical features related to gray-level co-occurrence matrices, including energy, contrast, correlation, and entropy, ADC, and DCE pharmacokinetic parameters: volume transfer constant (K^{trans}) and extravascular-extracellular volume fraction (V_e), were calculated from index tumors delineated on the T2w, DWI, and DCE-MRI, respectively. Energy and entropy correlated significantly ($P<0.05$) with both GS and median ADC. Contrast correlated moderately with median ADC. The textural features correlated insignificantly with K^{trans} and V_e. GS (4+3) cancers had significantly lower energy and higher entropy than 3+4 cancers, but insignificant differences in median ADC, K^{trans}, and V_e. The combined MRI radiomics parameters yielded higher classification accuracy (91%) than the individual parameter sets.

The last two papers in this section are algorithms that simultaneously identify the tumor lesion and assess the tumor aggressiveness. Tiwari *et al.* (52) combined radiomics information with metabolic data from MR spectroscopy (MRS) to develop a computerized decision support system. Features similar to Madabhushi *et al.* (45) were used.

Pollack *et al.* (53) developed a habitat risk scoring system for automatic delineation of the GTV. In their approach, the quantitative information from the diffusion and perfusion mpMRI is used to identify distinct pathophysiologic regions, called "Habitats" (59). An automated pixel by pixel method was optimized and associated with GS. The "Habitat Risk Score" (HRS) was devised in ten subcategories with increasing levels associated with a greater risk of harboring higher GS's and depicted as a heat map. HRS was related to radical prostatectomy (RP) tumor volumes and GS. The HRS algorithm had a higher sensitivity for detecting cancer

Table 4 Summary of radiomics manuscripts related to assessing the aggressiveness of the cancer

Reference	Volumes	Segmentation of tumor	Modality	Feature category*	Analysis endpoint
Wibmer *et al.*, 2015 (48)	ROI	Manual	T2w; ADC	Statistical	GS =6 *vs*. [GS (4+3) =7 and GS (3+4) =7]; GS =6 *vs*. GS ≥7; GS ≤3+4 *vs*. GS >3+4
Vignati *et al.*, 2015 (49)	ROI	Manual	T2w; ADC	Statistical	GS =6 *vs*. GS ≥7
Fehr *et al.*, 2016 (50)	ROI	Manual	T2w; ADC	Statistical	GS =6 *vs*. GS ≥7; GS (3+4) =7 *vs*. GS (4+3) =7
Nketiah *et al.*, 2017 (51)	ROI	Manual	T2w	Statistical	GS (3+4) =7 *vs*. GS (4+3) =7
Tiwari *et al.*, 2014 (52)	ROI	Automatic	T2w	Statistical; transform-based	[GS = (≤3+3) and GS = (3+4)] *vs*. [GS = (4+3) and GS = (4+4) and GS = (>4+4)]
Pollack *et al.*, 2017 (53)	ROI	Automatic	DCE-MRI; ADC	Statistical	Benign *vs*. GS ≥6; benign and GS =6 *vs*. GS ≥7; benign and GS =6 and GS =7 *vs*. GS ≥8

*, see *Table 1* for feature descriptions. NAT, normal appearing tissues; ROI, region of interest; GS, Gleason score; DCE, dynamic contrast enhanced; ADC, apparent diffusion coefficient; T2w, T2-weighted.

than PIRADS4/5: 45–100% for HRS4–9, compared to PIRADS' 25%. The volumes of HRS6 and RP ROIs were concordant (slope 1.09, r=0.767; P<0.0001). HRS6 provided an area under the curve (AUC) =0.718, 0.802 and 0.897 for predicting the likelihood of cancer, GS ≥7 and GS ≥8. By contrast, PIRADS had an AUC =0.62, 0.64 and 0.617. A workflow for RT planning was created in MIM where the HRS contours were migrated to the planning CT to define GTV. This is illustrated in *Figure 2*, where HRS6 map is used as GTV in the CT. HRS maps were created for the first 37 patients in an institutional phase II randomized clinical trial "MRI-Guided Prostate Boosts Via Initial Lattice Stereotactic vs Daily Moderately Hypofractionated Radiotherapy (BLaStM)" (http://clinicaltrials.gov: NCT02307058).

The promise of radiomics for treatment response

Radiomics of pre-treatment MRI

There are very few studies relating pre-RT radiomics with response to RT. In Ginsburg *et al.* (60) statistical and transform-based features related to GLIH, GLCOM and Gabor wavelet were extracted from T2w. To identify which of these texture features are potential independent prognostic markers of prostate-specific antigen (PSA) failure, the authors implemented a partial least squares (PLS) method to embed the data in a low dimensional space and then use the variable importance in projections method to quantify the contributions of individual features to classification on the PLS embedding. Three Gabor wavelet features were identified that, in conjunction with a logistic regression classifier, yielded AUC of 0.83 for predicting the probability of biochemical recurrence following RT. The presented evidence, albeit in a small cohort of 16 patients, suggests that radiomic features may capture micro-architecture in the tumors that provide morphometric information for predicting biochemical failure.

Gnep *et al.* (61) also investigated the association of radiomics and biochemical recurrence following RT. A retrospective cohort of 74 patients who underwent pre-treatment mpMRI were used. Median follow-up of 47 months revealed 11 patients with biochemical reoccurrence. Tumors were delineated on T2w and were propagated onto the co-registered ADC images. Twenty-eight T2w statistical features related to GLCOM and four morphological features (tumor diameter, perimeter, area, and volume) were found to be significantly associated with biochemical recurrence (P<0.05). The most relevant features were T2w contrast, T2w difference variance, ADC median, along with tumor volume and tumor area with Harrell's concordance index (C-index) from 0.76 to 0.82 (P<0.05). By combining these most powerful features in a random survival forest (RSF) model, the obtained C-index was 0.90. The results of the study revealed that GLCOM-based statistical features derived from T2w were strongly associated with biochemical recurrence, especially in the high-risk prostate cancer patients. Utilizing such parameters

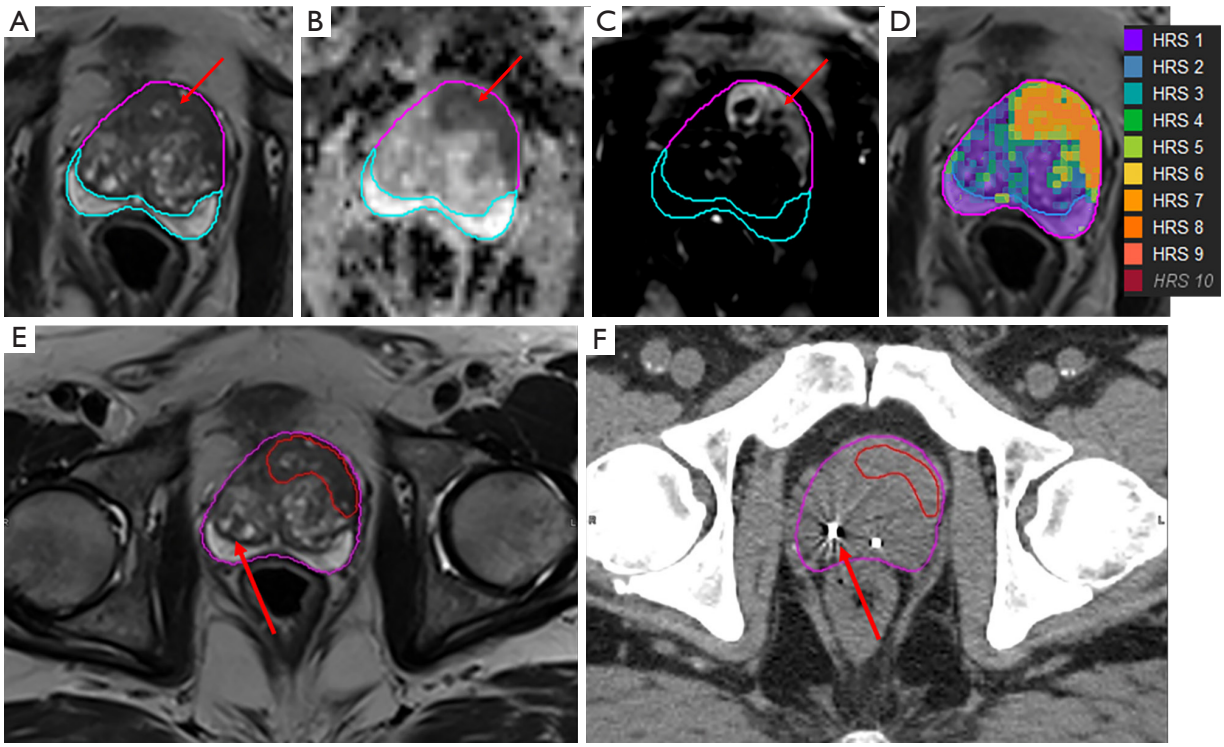

Figure 2 Implementation of Habitat Risk Score (HRS) in radiotherapy planning of a BLaStM patient. (A) An axial slice of the prostate on T2-weighted (T2w) MRI. The red arrow indicates an anterior tumor, characterized with hypo-intensity in the T2w; (B) corresponding slice of apparent diffusion coefficient (ADC) map with area of restricted diffusion (red arrow); (C) early enhancing image from the dynamic contrast enhanced (DCE)-MRI showing increased perfusion in the tumor area (red arrow); (D) Habitat Risk Score (HRS), represented as a heat-map, overlaid on the T2w. HRS is calculated in MIM, using Java plug-in. The approach scores every pixel with a 10-point scale (insert) in increasing risk for cancer. The volume of HRS10 is empty; (E) the 3D volume of the tumor, as depicted by HRS6 is used for gross tumor volume (GTV), the red arrow pointing to a fiducial marker; (F) the planning CT is aligned to the T2w, using fiducial matching (red arrow). The final result is displayed where the smoothed HRS6 contour has been migrated to the planning CT.

could have significant role in clinical decision-making process in future.

Delta-radiomics

Changes in radiomic features, called delta-radiomics, have been studied for their prognostic potentials in cancer management. The availability of longitude imaging studies pre-, during and post-RT provides a logical basis for delta-radiomics in RT. Currently, there are very few RT studies, mainly based on CT delta-radiomics. Cunliffe *et al.* (62) used delta-radiomics to identify a set of intensity and texture-based features related to radiation pneumonitis development for esophageal cancer patients. The authors analyzed the twenty texture features between pre- and after radiation therapy CT scans for all ROIs and found significant changes in twelve texture features with increasing radiation dose for patients who developed ≥2 radiation pneumonitis. However, this study was not able to determine the optimum set of texture features and model due to small patient size. A study by Fave *et al.* (63) investigated the change of radiomics features measured from CT images of non-small cell lung cancer (NSCLC) acquired at multiple time points during RT therapy for prediction of tumor response. In addition to delta-radiomics features obtained from the weekly 4D CT scans, this study incorporated clinical factors and pre-treatment radiomics features for prediction of patient outcome, including overall survival, freedom from distant metastases, and local-regional control. This study found that delta-radiomics were prognostic for overall survival although it did not offer substantially new prognostic information for distant metastases. For local-

regional recurrence, however, texture strength feature measured from the last week of 4D CT images was found to be predictive for outcome. The limitation of this study included the lack of independent model validation and use of median predicted value for the cut-off point of high- and low- risks patients.

Applying delta-radiomics approach to mpMRI is, however, challenging because of the numerous sequences, as well as the lack of outcome data for patients with contemporary mpMRI studies. There is also significant evidence that there is detectable radiomic signal pre- and post-RT. Based on preclinical studies, Lin *et al.* demonstrated that ADC values within the treated region of the tumor increased after RT compared with that of the untreated region (64). The authors implanted mice with cells from a transgenic adenocarcinoma of the mouse prostate (TRAMP)-C1 in order to investigate the biological meaning of changes within the ADC intensity values before and after RT. Intensity histogram analysis determined an increase in the entire normal distribution of the irradiated region as well as a decrease in kurtosis for that region, all coinciding with a decrease in pixel-by-pixel nuclear count with increased extracellular space and nuclear size. These ADCs were positively correlated with extracellular spaces and nuclear sizes while negatively correlating with nuclear counts, cytoplasmic space, and nuclear spaces. These changes are often associated with cell death pathways (decreased nuclear counts, increased extracellular space) and giant cell formation caused by disorganization of the mitotic spindle and incomplete mitosis (increased nuclear size). These studies, together with the maturing of the mpMRI data underscore the prospect of delta-radiomics for the development of new and powerful prediction models. However, it is important for such studies to focus on improving the standardization of texture features measured before treatment first and then correlating the values of texture features with biological and molecular characteristics as also suggested by Fave *et al.* (63).

Discussion

Although MRI-based radiomics shows great promise in cancer management, there are significant challenges. Unlike CT, MR image intensities do not necessarily reflect physical parameters like electron density, but vary with voxel size, magnetic field strength, pulse sequence, machine vendor and reconstruction algorithm (22). Several studies have investigated the dependence of radiomic textural features on MRI field strength, scanner manufacturer, and MRI acquisition parameters in both living subjects and phantoms (65-71). The basic strategy of radiomics is challenged by the wide range of image acquisition parameters and reconstruction algorithms among institutions and scanners (72). Thus, testing of MRI-based radiomic features for robustness and reproducibility is an important initial step in the radiomic workflow, and standardization of MR image acquisition across institutions should be encouraged.

Radiomics has the potential to describe tumor morphology using computer accessible imaging features that can be directly related to diagnosis or risk assessment. Dose escalation in radiation treatment of prostate cancer has been shown to reduce biochemical failure (9). While dose escalation also has been shown to reduce the need for androgen deprivation in intermediate to high risk patients, when the entire prostate is dose escalated, the complication risk rises (12,73,74). Dose escalation only to determinate prostate habitats has the potential to improve tumor control with less toxicity than when the entire prostate dose is escalated. The goal of the aforementioned ongoing BlaStM trial and other clinical trials at University of Miami is to evaluate various methods of increasing dose to the mpMRI-defined tumor region(s). In addition to treating the GTV, HRS is used to assign targets for the mpMRI-Ultrasound (MRI-US) fusion biopsy (75), aimed at generating data from MRI-US fusion biopsy pathology and gene expression. The rationale is that follow-up patient data (mpMRI at 3, 9 months and 2–2.5 years post-treatment) and biopsy at 2–2.5 years post-treatment will add additional information that may lead to better stratification, treatment, and prognosis of patients.

In conclusion, this review paper has summarized ongoing efforts to correlate radiomics features, acquired from prostate cancer MRI prior, during and after radiation treatment, to patient outcome. It should be stated that the concepts, methods and tools described herein are not currently applicable to the radiation oncology practice outside of the research setting. More data is required in the form of clinical trials to assess the robustness of radiomics-based predictive models, and to maximize the efficacy of these models. As medical imaging scientists and radiation oncology physicians grow more comfortable with integrating radiomics and into clinical decision-making, we believe this important innovation has the potential to provide a significant step toward the goal of personalized

patient care for prostate cancer.

Acknowledgements

Funding: This work was funded by the National Institutes of Health (grant numbers R01CA189295, R01CA190105).

Footnote

Conflicts of Interest: The authors have no conflicts of interest to declare.

References

1. Siegel RL, Miller KD, Jemal A. Cancer statistics, 2018. CA Cancer J Clin 2018;68:7-30.
2. Crook JM, Malone S, Perry G, et al. Twenty-Four-Month Postradiation Prostate Biopsies Are Strongly Predictive of 7-Year Disease-free Survival. Cancer 2009;115:673-9.
3. Vance W, Tucker SL, De Crevoisier R, et al. The predictive value of 2-year posttreatment biopsy after prostate cancer radiotherapy for eventual biochemical outcome. Int J Radiat Oncol Biol Phys 2007;67:828-33.
4. Zelefsky MJ, Reuter VE, Fuks Z, et al. Influence of local tumor control on distant metastases and cancer related mortality after external, beam radiotherapy for prostate cancer. J. Urol 2008;179:1368-73.
5. Arrayeh E, Westphalen AC, Kurhanewicz J, et al. Does local recurrence of prostate cancer after radiation therapy occur at the site of primary tumor? Results of a longitudinal MRI and MRSI study. Int J Radiat Oncol Biol Phys 2012;82:e787-93.
6. Buyyounouski MK, Li T, Al-Saleem T, et al. Predicting local persistence of intermediate and high-risk prostate cancer using percentage of adenocarcinoma in pretreatment biopsy tissue. Int J Radiat Oncol 2008;72:S321-2.
7. Chopra S, Toi A, Taback N, et al. Pathological Predictors for Site of Local Recurrence After Radiotherapy for Prostate Cancer. Int J Radiat Oncol Biol Phys 2012;82:e441-8.
8. Eade TN, Hanlon AL, Horwitz EM, et al. What dose of external-beam radiation is high enough for prostate cancer? Int J Radiat Oncol Biol Phys 2007;68:682-9.
9. Kuban DA, Levy LB, Cheung MR, et al. Long-Term Failure Patterns and Survival in a Randomized Dose-Escalation Trial for Prostate Cancer. Who Dies of Disease? Int J Radiat Oncol Biol Phys 2011;79:1310-7.
10. Morris WJ, Tyldesley S, Rodda S, et al. Androgen Suppression Combined with Elective Nodal and Dose Escalated Radiation Therapy (the ASCENDE-RT Trial): An Analysis of Survival Endpoints for a Randomized Trial Comparing a Low-Dose-Rate Brachytherapy Boost to a Dose-Escalated External Beam Boost for High- and Intermediate-risk Prostate Cancer. Int J Radiat Oncol Biol Phys 2017;98:275-85.
11. Pucar D, Hricak H, Shukla-Dave A, et al. Clinically significant prostate cancer local recurrence after radiation therapy occurs at the site of primary tumor: magnetic resonance imaging and step-section pathology evidence. Int J Radiat Oncol Biol Phys 2007;69:62-9.
12. Bauman G, Haider M, Van der Heide UA, et al. Boosting imaging defined dominant prostatic tumors: A systematic review. Radiother Oncol 2013;107:274-81.
13. Lips IM, van der Heide UA, Haustermans K, et al. Single blind randomized phase III trial to investigate the benefit of a focal lesion ablative microboost in prostate cancer (FLAME-trial): study protocol for a randomized controlled trial. Trials 2011;12:255.
14. von Eyben FE, Kiljunen T, Kangasmaki A, et al. Radiotherapy Boost for the Dominant Intraprostatic Cancer Lesion-A Systematic Review and Meta-Analysis. Clin Genitourin Cancer 2016;14:189-97.
15. Feutren T, Herrera FG. Prostate irradiation with focal dose escalation to the intraprostatic dominant nodule: a systematic review. Prostate International 2018. Available online: https://doi.org/10.1016/j.prnil.2018.03.005
16. Nichol AM, Warde P, Bristow RG. Optimal treatment of intermediate-risk prostate carcinoma with radiotherapy: clinical and translational issues. Cancer 2005;104:891-905.
17. Buyyounouski MK, Pickles T, Kestin LL, et al. Validating the interval to biochemical failure for the identification of potentially lethal prostate cancer. J Clin Oncol 2012;30:1857-63.
18. Isebaert S, Van den Bergh L, Haustermans K, et al. Multiparametric MRI for prostate cancer localization in correlation to whole-mount histopathology. J Magn Reson Imaging 2013;37:1392-401.
19. Fütterer JJ, Briganti A, De Visschere P, et al. Can Clinically Significant Prostate Cancer Be Detected with Multiparametric Magnetic Resonance Imaging? A Systematic Review of the Literature. Eur Urol 2015;68:1045-53.
20. Barentsz JO, Richenberg J, Clements R, et al. ESUR

prostate MR guidelines 2012. Eur Radiol 2012;22:746-57.
21. Weinreb JC, Barentsz JO, Choyke PL, et al. PI-RADS Prostate Imaging - Reporting and Data System: 2015, Version 2. Eur Urol 2016;69:16-40.
22. Kumar V, Gu Y, Basu S, et al. Radiomics: the process and the challenges. Magn Reson Imaging 2012;30:1234-48.
23. Lambin P, Rios-Velazquez E, Leijenaar R, et al. Radiomics: extracting more information from medical images using advanced feature analysis. Eur J Cancer 2012;48:441-6.
24. Aerts HJ, Velazquez ER, Leijenaar RT, et al. Decoding tumour phenotype by noninvasive imaging using a quantitative radiomics approach. Nat Commun 2014;5:4006. Erratum in: Nat Commun 2014;5:4644. Cavalho, Sara [corrected to Carvalho, Sara].
25. Gillies RJ, Kinahan PE, Hricak H. Radiomics: Images Are More than Pictures, They Are Data. Radiology 2016;278:563-77.
26. Stoyanova R, Takhar M, Tschudi Y, et al. Prostate cancer radiomics and the promise of radiogenomics. Transl Cancer Res 2016;5:432-47.
27. Yang F, Thomas M, Dehdashti F, et al. Temporal analysis of intratumoral metabolic heterogeneity characterized by texture features in cervical cancer. Eur J Nucl Med Mol Imaging 2013;40:716-27.
28. Avanzo M, Stancanello J, El Naqa I. Beyond imaging: The promise of radiomics. Phys Med 2017;38:122-39.
29. Yip SS, Aerts H. Applications and limitations of radiomics. Phys Med Biol 2016;61:R150-66.
30. Yang F, Young L, Grigsby P. Predictive value of standardized intratumoral metabolic heterogeneity in locally advanced cervical cancer treated with chemoradiation. Int J Gynecol Cancer 2016;26:777-84.
31. Scalco E, Fiorino C, Cattaneo GM, et al. Texture analysis for the assessment of structural changes in parotid glands induced by radiotherapy. Radiother Oncol 2013;109:384-7.
32. Court LE, Fave X, Mackin D, et al. Computational resources for radiomics. Transl Cancer Res 2016;5:340-8.
33. Hoeks CM, Hambrock T, Yakar D, et al. Transition zone prostate cancer: detection and localization with 3-T multiparametric MR imaging. Radiology 2013;266:207-17.
34. Johnson LM, Turkbey B, Figg WD, et al. Multiparametric MRI in prostate cancer management. Nat Rev Clin Oncol 2014;11:346-53.
35. Johnson PB, Young L, Lamichhane N, et al. Quantitative imaging: correlating image features with the segmentation accuracy of PET based tumor contours in the lung. Radiother Oncol 2017;123:257-62.
36. Mecke KR. Additivity, Convexity, and Beyond: Applications of Minkowski Functionals in Statistical Physics. In: Mecke KR, Stoyan D. editors. Statistical Physics and Spatial Statistics. Lecture Notes in Physics, vol 554. Springer, Berlin, Heidelberg, 2000.
37. Lopes R, Ayache A, Makni N, et al. Prostate cancer characterization on MR images using fractal features. Med Phys 2011;38:83-95.
38. Haralick RM. Statistical and structural approaches to texture. Proc. IEEE 1979;67:786-804.
39. Amadasun M, King R. Textural features corresponding to textural properties. IEEE Trans Syst Man Cybern Syst 1989;19:1264-74.
40. Thibault G, Fertil B, Navarro C, et al. Texture indexes and gray level size zone matrix: application to cell nuclei classification. Paper presented at: Pattern Recognition and Information Processing, 2009.
41. Loh HH, Leu JG, Luo RC. The analysis of natural textures using run length features. IEEE Trans Ind Electron 1988;35:323-8.
42. Bigun J. Speed, frequency, and orientation tuned 3-D Gabor filter banks and their design. Pattern Recognition, 1994. Vol. 3 - Conference C: Signal Processing, Proceedings of the 12th IAPR International Conference on.
43. Ganeshan B, Miles KA, Young RC, et al. Three-dimensional selective-scale texture analysis of computed tomography pulmonary angiograms. Invest Radiol 2008;43:382-94.
44. Mallat S. A wavelet tour of signal processing. Academic press, 1999.
45. Madabhushi A, Feldman MD, Metaxas DN, et al. Automated detection of prostatic adenocarcinoma from high-resolution ex vivo MRI. IEEE Trans Med Imaging 2005;24:1611-25.
46. Cameron A, Khalvati F, Haider MA, et al. MAPS: A Quantitative Radiomics Approach for Prostate Cancer Detection. IEEE Trans Biomed Eng 2016;63:1145-56.
47. Shiradkar R, Podder TK, Algohary A, et al. Radiomics based targeted radiotherapy planning (Rad-TRaP): a computational framework for prostate cancer treatment planning with MRI. Radiat Oncol 2016;11:148.
48. Wibmer A, Hricak H, Gondo T, et al. Haralick texture analysis of prostate MRI: utility for differentiating non-cancerous prostate from prostate cancer and differentiating prostate cancers with different Gleason scores. Eur Radiol 2015;25:2840-50.
49. Vignati A, Mazzetti S, Giannini V, et al. Texture features

on T2-weighted magnetic resonance imaging: new potential biomarkers for prostate cancer aggressiveness. Phys Med Biol 2015;60:2685-701.
50. Fehr D, Veeraraghavan H, Wibmer A, et al. Automatic classification of prostate cancer Gleason scores from multiparametric magnetic resonance images. Proc Natl Acad Sci U S A 2015;112:E6265-73.
51. Nketiah G, Elschot M, Kim E, et al. T2-weighted MRI-derived textural features reflect prostate cancer aggressiveness: preliminary results. Eur Radiol 2017;27:3050-9.
52. Tiwari P, Kurhanewicz J, Madabhushi A. Multi-kernel graph embedding for detection, Gleason grading of prostate cancer via MRI/MRS. Med Image Anal 2013;17:219-35.
53. Pollack A, Abramowitz MC, Kwon D, et al. An Automated Multiparametric MRI Quantitative Imaging Prostate Habitat Risk Scoring System for Defining External Beam Radiation Therapy Boost Volumes. Int J Radiat Oncol Biol Phys 2017;99:S50-1.
54. Lv D, Guo X, Wang X, et al. Computerized characterization of prostate cancer by fractal analysis in MR images. J Magn Reson Imaging 2009;30:161-8.
55. Kwak JT, Xu S, Wood BJ, et al. Automated prostate cancer detection using T2-weighted and high-b-value diffusion-weighted magnetic resonance imaging. Med Phys 2015;42:2368-78.
56. Khalvati F, Wong A, Haider MA. Automated prostate cancer detection via comprehensive multi-parametric magnetic resonance imaging texture feature models. BMC Med Imaging 2015;15:27.
57. Litjens GJS, Elliott R, Shih N, et al. Distinguishing prostate cancer from benign confounders via a cascaded classifier on multi-parametric MRI. Proc SPIE 9035, Medical Imaging 2014: Computer-Aided Diagnosis, 903512 (18 March 2014). doi: 10.1117/12.2043751.
58. Litjens GJS, Elliott R, Shih NNC, et al. Computer-extracted Features Can Distinguish Noncancerous Confounding Disease from Prostatic Adenocarcinoma at Multiparametric MR Imaging. Radiology 2016;278:135-45.
59. Gatenby RA, Grove O, Gillies RJ. Quantitative imaging in cancer evolution and ecology. Radiology 2013;269:8-15.
60. Ginsburg SB, Rusu M, Kurhanewicz J, et al. Computer extracted texture features on T2w MRI to predict biochemical recurrence following radiation therapy for prostate cancer. Proc SPIE 9035, Medical Imaging 2014: Computer-Aided Diagnosis, 903509 (24 March 2014). doi: 10.1117/12.2043937.
61. Gnep K, Fargeas A, Gutierrez-Carvajal RE, et al. Haralick textural features on T2 -weighted MRI are associated with biochemical recurrence following radiotherapy for peripheral zone prostate cancer. J Magn Reson Imaging 2017;45:103-17.
62. Cunliffe A, Armato SG 3rd, Castillo R, et al. Lung texture in serial thoracic computed tomography scans: correlation of radiomics-based features with radiation therapy dose and radiation pneumonitis development. Int J Radiat Oncol Biol Phys 2015;91:1048-56.
63. Fave X, Zhang L, Yang J, et al. Delta-radiomics features for the prediction of patient outcomes in non-small cell lung cancer. Sci Rep 2017;7:588.
64. Lin YC, Lin G, Hong JH, et al. Diffusion radiomics analysis of intratumoral heterogeneity in a murine prostate cancer model following radiotherapy: Pixelwise correlation with histology. J Magn Reson Imaging 2017;46:483-9.
65. Herlidou-Même S, Constans JM, Carsin B, et al. MRI texture analysis on texture test objects, normal brain and intracranial tumors. Magn Reson Imaging 2003;21:989-93.
66. Jirák D, Dezortova M, Hajek M. Phantoms for texture analysis of MR images. Long-term and multi-center study. Med Phys 2004;31:616-22.
67. Mayerhoefer ME, Szomolanyi P, Jirak D, et al. Effects of MRI acquisition parameter variations and protocol heterogeneity on the results of texture analysis and pattern discrimination: An application-oriented study. Med Phys 2009;36:1236-43.
68. Yang F, Ford J, Dogan N. Impact of Pulse Sequence Selection on T1-weighted MRI Radiomic Textural Features. Med Phys 2017;44:2812.
69. Yang F, Ford J, Dogan N. Validation of Quantitative Radiomic Texture Features for Oncologic MRI: A Simulation Study. Med Phys 2016;43:3386.
70. Savio SJ, Harrison LC, Luukkaala T, et al. Effect of slice thickness on brain magnetic resonance image texture analysis. Biomed Eng Online 2010;9:60.
71. Waugh SA, Lerski RA, Bidaut L, et al. The influence of field strength and different clinical breast MRI protocols on the outcome of texture analysis using foam phantoms. Med Phys 2011;38:5058-66.
72. Summers RM. Texture analysis in radiology: Does the emperor have no clothes? Abdom Radiol (NY) 2017;42:342-5.
73. Demanes DJ, Brandt D, Schour L, et al. Excellent results from high dose rate brachytherapy and external beam for

prostate cancer are not improved by androgen deprivation. Am J Clin Oncol 2009;32:342-7.
74. Dattoli M, Wallner K, True L, et al. Long-term outcomes for patients with prostate cancer having intermediate and high-risk disease, treated with combination external beam irradiation and brachytherapy. J Oncol 2010;2010. doi: 10.1155/2010/471375.
75. Sandler K, Patel M, Lynne C, et al. Multiparametric-MRI and targeted biopsies in the management of prostate cancer patients on active surveillance. Front Oncol 2015;5:4.

Cite this article as: Yang F, Ford JC, Dogan N, Padgett KR, Breto AL, Abramowitz MC, Dal Pra A, Pollack A, Stoyanova R. Magnetic resonance imaging (MRI)-based radiomics for prostate cancer radiotherapy. Transl Androl Urol 2018;7(3):445-458. doi: 10.21037/tau.2018.06.05

